

Computational inverse scattering with internal sources: a reproducing kernel Hilbert space approach

Y. Dong, K. Sadiq, O. Scherzer,
J.C. Schotland

RICAM-Report 2024-16

Computational inverse scattering with internal sources: a reproducing kernel Hilbert space approach

Yakun Dong¹

yakun.dong@univie.ac.at

Kamran Sadiq²

Kamran.Sadiq@oeaw.ac.at

Otmar Scherzer^{1,2,3}

otmar.scherzer@univie.ac.at

John C. Schotland⁴

john.schotland@yale.edu

¹Faculty of Mathematics
University of Vienna
Oskar-Morgenstern-Platz 1
A-1090 Vienna, Austria

²Johann Radon Institute for Computational
and Applied Mathematics (RICAM)
Altenbergerstraße 69
A-4040 Linz, Austria

³Christian Doppler Laboratory for Mathematical
Modeling and Simulation of Next Generations
of Ultrasound Devices (MaMSi)
Oskar-Morgenstern-Platz 1
A-1090 Vienna, Austria

⁴Department of Mathematics and
Department of Physics
Yale University
New Haven, CT 06520-8283, USA

ABSTRACT

We present a method to reconstruct the dielectric susceptibility (scattering potential) of an inhomogeneous scattering medium, based on the solution to the inverse scattering problem with internal sources. We consider a scalar model of light propagation in the medium. We employ the theory of reproducing kernel Hilbert spaces, together with regularization to recover the susceptibility of two- and three-dimensional scattering media. Numerical examples illustrate the effectiveness of the proposed reconstruction method.

1. INTRODUCTION

The inverse scattering problem is concerned with determining the structure of a scattering medium from measurements of the scattered field. Such problems have numerous applications including medical imaging, nondestructive testing, remote and radar sensing, ocean acoustics and geophysical exploration; see e.g. [13, 7, 22, 4], and the references therein.

In this paper, we investigate an inverse scattering problem with internal sources and show that it is possible to recover the dielectric susceptibility (scattering potential) of an inhomogeneous scattering medium. Suitable internal sources take the form of photoactivated fluorophores, which are used in superresolution microscopy [2, 10], and subwavelength bubbles, which are used in ultrasound localization microscopy [8]. The considered inverse problem is ill-posed. We apply the theory of reproducing kernel Hilbert spaces (RKHS) [1, 12] accompanied by tools from regularization theory (see e.g. [21, 6]) to reconstruct the susceptibility.

In [9], a similar inverse problem is considered, also using an integral equation approach. The integral equation is converted into a linear system of algebraic equations, which is solved by means of a regularized pseudoinverse to recover the susceptibility. Instead, here we use the RKHS approach, which yields reconstructed images of higher quality compared to [9].

This paper is organized as follows. In Section 2, we formulate the forward problem and the associated inverse scattering problem. We also briefly recall some tools from the theory of regularization and RKHS, which we need for our reconstruction method. In addition, we present the method for both two- and three-dimensional inverse problems. In Section 3, we present the results obtained by applying the RKHS reconstruction method to three numerical experiments. We also present some comparison results to [9], as shown in Table 1. Finally, in Section 4, we present our concluding remarks.

2. INVERSE SCATTERING PROBLEM WITH INTERNAL SOURCES

We consider an experiment in which light from a monochromatic source propagates in an inhomogeneous medium in two dimensions. The three-dimensional case is taken up in Section 2.3. The source is taken to be located in the interior of the medium and to consist of a single photoactivated fluorescent molecule. The scattered light is then registered by a detector in the far field for each source. For simplicity, we consider a scalar model of the optical field, in the form of the time-harmonic wave equation,

$$\Delta U(\mathbf{r}) + k^2(1 + \eta(\mathbf{r}))U(\mathbf{r}) = -a(\mathbf{r}_1)\delta(\mathbf{r} - \mathbf{r}_1), \quad (2.1)$$

where U is the field, $\eta(\mathbf{r})$ is the susceptibility of the medium at the position \mathbf{r} , and k is the wave number. Since the source consists of a single molecule, it is taken to be a point source with position \mathbf{r}_1 and amplitude $a(\mathbf{r}_1)$. This model does not account for the transversality of the electric field and is often used in physical optics [3]. A vector theory of the electromagnetic field, which allows for the effects of polarization, will be explored in future work.

The total field may be decomposed into the incident field U_i and scattered field U_s . Following standard procedure [4, 3], the total field satisfies the integral equation

$$U(\mathbf{r}) = U_i(\mathbf{r}) + k^2 \int G(\mathbf{r}, \mathbf{r}')\eta(\mathbf{r}')U(\mathbf{r}')d\mathbf{r}', \quad (2.2)$$

where

$$G(\mathbf{r}, \mathbf{r}') := \frac{i}{4}H_0^{(1)}(k|\mathbf{r} - \mathbf{r}'|) \quad (2.3)$$

is the two-dimensional Green's function, with $H_0^{(1)}$ being the Hankel function of first kind [5]. The Green's function satisfies the equation

$$\Delta_{\mathbf{r}}G(\mathbf{r}, \mathbf{r}') + k^2G(\mathbf{r}, \mathbf{r}') = -\delta(\mathbf{r} - \mathbf{r}'), \quad (2.4)$$

together with the Sommerfeld radiation condition [5].

In the far-zone, the Hankel function has the asymptotic form, see e.g. [5, Section 3.4 (3.59)]:

$$\frac{i}{4}H_0^{(1)}(kR) \sim \frac{e^{i\frac{\pi}{2}}}{4} \sqrt{\frac{2}{\pi kR}} e^{-\frac{\pi}{4}i} e^{ikR} = \frac{e^{i\frac{\pi}{4}}}{\sqrt{8\pi k}} \frac{e^{ikR}}{\sqrt{R}}, \quad (2.5)$$

which propagates as a cylindrical wave with amplitude $R^{-1/2}$. Thus, in the far field, we obtain the asymptotic formula for the two-dimensional Green's function,

$$\begin{aligned} G(\mathbf{r}, \mathbf{r}') &= \frac{i}{4}H_0^{(1)}(k|\mathbf{r} - \mathbf{r}'|) \sim \frac{e^{i\frac{\pi}{4}}}{\sqrt{8\pi k}} \frac{e^{ik|\mathbf{r} - \mathbf{r}'|}}{\sqrt{|\mathbf{r} - \mathbf{r}'|}} \\ &\simeq \frac{e^{i\frac{\pi}{4}}}{\sqrt{8\pi k}} \frac{e^{ik|\mathbf{r}|}}{\sqrt{|\mathbf{r}|}} e^{-ik\hat{\mathbf{r}} \cdot \mathbf{r}'} \left(1 + \frac{1}{2} \frac{\hat{\mathbf{r}} \cdot \mathbf{r}'}{|\mathbf{r}|}\right). \end{aligned} \quad (2.6)$$

Since the incident field is given by $U_i(\mathbf{r}) = a(\mathbf{r}_1)G(\mathbf{r}, \mathbf{r}_1)$, we derive by using (2.6) the asymptotic behavior of the total field,

$$\begin{aligned} U(\mathbf{r}) &= a(\mathbf{r}_1)G(\mathbf{r}, \mathbf{r}_1) + k^2 \int G(\mathbf{r}, \mathbf{r}')\eta(\mathbf{r}')U(\mathbf{r}')d\mathbf{r}' \\ &\sim \frac{e^{i\frac{\pi}{4}}}{\sqrt{8\pi}} \frac{e^{ik|\mathbf{r}|}}{\sqrt{|\mathbf{r}|}} \left(\frac{a(\mathbf{r}_1)}{\sqrt{k}} e^{-ik\hat{\mathbf{r}} \cdot \mathbf{r}_1} + k^{\frac{3}{2}} \int e^{-ik\hat{\mathbf{r}} \cdot \mathbf{r}'}\eta(\mathbf{r}')U(\mathbf{r}')d\mathbf{r}' \right). \end{aligned}$$

Thus, in the far zone of the scatterer, the field behaves as an outgoing cylindrical wave:

$$U(\mathbf{r}) \sim \frac{e^{i\frac{\pi}{4}}}{\sqrt{8\pi}} \frac{e^{ik|\mathbf{r}|}}{\sqrt{|\mathbf{r}|}} \left(\frac{a(\mathbf{r}_1)}{\sqrt{k}} e^{-ik\hat{\mathbf{r}} \cdot \mathbf{r}_1} + A(\mathbf{r}) \right), \quad (2.7)$$

where the scattering amplitude A is defined by

$$A(\mathbf{r}) := k^{\frac{3}{2}} \int_{\Omega} e^{-ik\hat{\mathbf{r}} \cdot \mathbf{r}'}\eta(\mathbf{r}')U(\mathbf{r}')d\mathbf{r}', \quad (2.8)$$

and Ω is the volume of the scatterer.

In the weak-scattering approximation, the scattering amplitude can be calculated by replacing U with U_i . Since the scattering amplitude A is recorded in the far zone at the point \mathbf{r}_2 , the scattering amplitude can be rewritten as:

$$A(\mathbf{r}_1, \mathbf{r}_2) = a(\mathbf{r}_1)k^{\frac{3}{2}} \int_{\Omega} e^{-ik\hat{\mathbf{r}}_2 \cdot \mathbf{r}} \eta(\mathbf{r}) G(\mathbf{r}, \mathbf{r}_1) d\mathbf{r}, \quad (2.9)$$

where the dependence of the scattering amplitude $A(\mathbf{r}_1, \mathbf{r}_2)$ on the source position \mathbf{r}_1 and the detector position \mathbf{r}_2 has been made explicit. The inverse problem thus consists of solving the integral equation (2.9) to recover the susceptibility η .

If we differentiate (2.9) with respect to \mathbf{r}_1 , use (2.4) and assume the sources have unit amplitude, we obtain

$$\begin{aligned} \Delta_{\mathbf{r}_1} A(\mathbf{r}_1, \mathbf{r}_2) + k^2 A(\mathbf{r}_1, \mathbf{r}_2) &= k^{\frac{3}{2}} \int_{\Omega} e^{-ik\hat{\mathbf{r}}_2 \cdot \mathbf{r}} \eta(\mathbf{r}) (\Delta_{\mathbf{r}_1} G(\mathbf{r}, \mathbf{r}_1) + k^2 G(\mathbf{r}, \mathbf{r}_1)) d\mathbf{r} \\ &= k^{\frac{3}{2}} \int_{\Omega} e^{-ik\hat{\mathbf{r}}_2 \cdot \mathbf{r}} \eta(\mathbf{r}) (-\delta(\mathbf{r} - \mathbf{r}_1)) d\mathbf{r} = -k^{\frac{3}{2}} e^{-ik\hat{\mathbf{r}}_2 \cdot \mathbf{r}_1} \eta(\mathbf{r}_1). \end{aligned}$$

We thus obtain an inversion formula for η of the form

$$\eta(\mathbf{r}_1; \mathbf{r}_2) = -\frac{e^{ik\hat{\mathbf{r}}_2 \cdot \mathbf{r}_1}}{k^{\frac{3}{2}}} (\Delta_{\mathbf{r}_1} A(\mathbf{r}_1, \mathbf{r}_2) + k^2 A(\mathbf{r}_1, \mathbf{r}_2)). \quad (2.10)$$

Theoretically, the susceptibility η depends only on the position of the sources \mathbf{r}_1 and is independent of the position of the detectors \mathbf{r}_2 . Thus, a single detector is sufficient for the reconstruction. However, due to the noise in numerical simulations, multiple detectors are often used to capture the scattering amplitude, leading to multiple reconstructions of η . To distinguish these, we denote them as $\eta(\mathbf{r}_1; \mathbf{r}_2)$. Next, we determine the dependence of η solely on the source positions \mathbf{r}_1 by averaging the reconstructions:

$$\eta(\mathbf{r}_1) = \frac{\sum_{\mathbf{r}_2} \eta(\mathbf{r}_1; \mathbf{r}_2)}{n_d}, \quad (2.11)$$

where n_d represents the number of detectors.

We illustrate the proposed reconstruction method in both two-dimensional and three-dimensional scattering media (see subsection 2.3 below). To avoid any ambiguity, we call the inversion of the susceptibility in a two-dimensional medium as the two-dimensional reconstruction method, while the inversion in a three-dimensional medium is called the three-dimensional reconstruction method.

2.1. Numerical analysis of the forward problem. We begin with the numerical analysis of the forward problem. Since the scattering amplitude is computed from (2.9) and there is a logarithmic singularity in the two-dimensional Green's function, a careful evaluation of the integral is required. To proceed, we discretize Ω into pixels C_m ($m = 1, 2, \dots, N_\nu$) of area h^2 , where N_ν is the total number of pixels. Assuming unit amplitude $a = 1$ for all sources, we split the integral of (2.9) into singular- and non-singular parts:

$$\int_{\Omega} e^{-ik\hat{\mathbf{r}}_2 \cdot \mathbf{r}} \eta(\mathbf{r}) G(\mathbf{r}, \mathbf{r}_1) d\mathbf{r} = \sum_{m=1}^{N_\nu} \int_{C_m \setminus C_n} e^{-ik\hat{\mathbf{r}}_2 \cdot \mathbf{r}} \eta(\mathbf{r}) G(\mathbf{r}, \mathbf{r}_1) d\mathbf{r} + \int_{C_n} e^{-ik\hat{\mathbf{r}}_2 \cdot \mathbf{r}} \eta(\mathbf{r}) G(\mathbf{r}, \mathbf{r}_1) d\mathbf{r}, \quad (2.12)$$

where C_n is the pixel containing the singularity. We assume that $kh \ll 1$. As the non-singular part can be computed directly, the singular part remains to be estimated.

The Green's function $G(\mathbf{r}, \mathbf{r}')$ is weakly singular at $\mathbf{r} = \mathbf{r}'$. We will approximate the two-dimensional Green's function near the singularity using its asymptotic form:

$$G(\mathbf{r}, \mathbf{r}') = \frac{1}{2\pi} \ln \frac{1}{|\mathbf{r} - \mathbf{r}'|} + \frac{i}{4} - \frac{\gamma}{2\pi} - \frac{1}{2\pi} \ln \frac{k}{2} + O\left(|\mathbf{r} - \mathbf{r}'|^2 \ln \frac{1}{|\mathbf{r} - \mathbf{r}'|}\right), \quad (2.13)$$

for $|\mathbf{r} - \mathbf{r}'| \rightarrow 0$, where $\gamma = 0.5772156$ is the Euler-Mascheroni constant. Thus, the singular part in (2.12) can be computed as

$$\int_{C_n} \eta(\mathbf{r}) e^{-ik\hat{\mathbf{r}}_2 \cdot \mathbf{r}} G(\mathbf{r}, \mathbf{r}_1) d\mathbf{r} \approx \eta(\tilde{\mathbf{r}}) e^{-ik\hat{\mathbf{r}}_2 \cdot \tilde{\mathbf{r}}} \frac{h^2}{2\pi} \left(\xi - \ln \frac{hk}{2} \right),$$

where $\xi = \frac{1}{2}(3 + \ln 2) - \frac{\pi}{4} - \gamma + \frac{i\pi}{2}$ and $\tilde{\mathbf{r}}$ is the central point in pixel C_n .

2.2. Numerical analysis of the inverse problem. Next, we focus on estimating the susceptibility through differentiation of the measured scattering amplitude A using (2.10). We apply the theory of RKHS [1, 12], to carry out the indicated differentiation, which allows for an explicit formulation of a functional by means of a reproducing kernel [20, 18].

To ensure the necessary smoothness, we choose the standard Sobolev space $\mathcal{W} = W_2^s(\mathbb{R}^d)$, where $d = 4$ and $s = 3$. In this case, the Sobolev embedding theorem is satisfied for $s > d/2$. This condition implies that \mathcal{W} is a space of continuous functions, and the function values are continuous linear functionals, indicating that it is a reproducing kernel Hilbert space. The reproducing kernel of the Sobolev space $W_2^3(\mathbb{R}^4)$ is given by [17]:

$$\kappa(\mathbf{x}, \mathbf{t}) = \int_{\mathbb{R}^4} \frac{\prod_{j=1}^4 \cos(2\pi(x_j - t_j)u_j)}{(1 + \sum_{0 < |\alpha|_1 \leq 3} \prod_{j=1}^4 (2\pi u_j)^{2\alpha_j})} d\mathbf{u}, \quad (2.14)$$

for all $\mathbf{x} = (x_1, \dots, x_4), \mathbf{t} = (t_1, \dots, t_4) \in \mathbb{R}^4$, where $|\alpha|_1 = \sum_{j=1}^4 \alpha_j$ with non-negative integers α_j .

The reproducing kernel we use from [17] is in a real Sobolev space \mathcal{W} . To approximate the scattering amplitude A which is complex-valued, we can identify a complex functional in $\mathcal{H} := \mathcal{W} \oplus i\mathcal{W}$, a complex linear space. It follows that we must show that \mathcal{H} is a RKHS space, which entails proving that the evaluation functionals are continuous. We can then make use of the result that a Hilbert space is a RKHS if and only if the evaluation functional is continuous. To proceed, we separate A into its real and imaginary parts and approximate the real and imaginary parts separately. We must then identify real functionals $f \approx \Re A$ and $\psi \approx \Im A$ in the real RKHS \mathcal{W} . In turn we then approximate A by a functional in \mathcal{H} by $A \approx F := f + i\psi$. This approach makes it possible to use a reproducing kernel for the real Sobolev space \mathcal{W} , circumventing the above issue.

Let \mathcal{D} be the set of all of the possible $(\mathbf{r}_1, \mathbf{r}_2)$, where \mathbf{r}_1 and \mathbf{r}_2 denote the positions of the sources and detectors, respectively, and let $\mathbf{x} = (\mathbf{r}_1, \mathbf{r}_2) \in \mathbb{R}^4$. In the setting of our problem, let $\bar{A}_i = \Re A(\mathbf{x}_i)$ and $\hat{A}_i = \Im A(\mathbf{x}_i)$ for every $\mathbf{x}_i \in \mathcal{D}$, then it follows that we need to find $f(\mathbf{x}_i)$ to approximate \bar{A}_i and $\psi(\mathbf{x}_i)$ to approximate \hat{A}_i separately. This leads to the following two optimization problems:

$$\operatorname{argmin}_f \frac{1}{n} \sum_{i=1}^n |\bar{A}_i - f(\mathbf{x}_i)|^2 + \lambda_1 \|f\|_{\mathcal{W}}^2, \quad (2.15)$$

$$\operatorname{argmin}_\psi \frac{1}{n} \sum_{i=1}^n |\hat{A}_i - \psi(\mathbf{x}_i)|^2 + \lambda_2 \|\psi\|_{\mathcal{W}}^2, \quad (2.16)$$

where $n = n_s \times n_d$, with n_s the number of sources, n_d the number of detectors, and $0 < \lambda_1, \lambda_2$ are suitable regularization parameters.

The optimization problems (2.15) and (2.16) have the same form. For convenience, we only describe the analysis of (2.15).

The following result (commonly referred as the representer theorem [12, 11]) demonstrates that the minimizer of problem (2.15) still lies in the space \mathcal{W} under certain conditions. This result effectively reduces the original infinite-dimensional minimization problem (2.15) to a finite-dimensional one for the scalar coefficients. More precisely, if the space \mathcal{W} has a reproducing kernel $\kappa : X \times X \rightarrow \mathbb{R}$, then the minimizer f^* of the problem (2.15) lies in a finite-dimensional subspace of the infinite-dimensional space \mathcal{W} , where

$$f^*(\cdot) = \sum_{i=1}^n c_i^* \kappa(\mathbf{x}_i, \cdot), \quad c_i^* \in \mathbb{R}, \quad (2.17)$$

and $\mathbf{x}_i \in \mathcal{D}$ is the known input.

Let K be the Gram matrix, with $K_{i,j} = \kappa(\mathbf{x}_i, \mathbf{x}_j)$, where $\mathbf{x}_i, \mathbf{x}_j \in \mathcal{D}$. Then any functional $f \in \operatorname{span}\{\kappa(\mathbf{x}_i, \cdot), i = 1, 2, \dots, n\}$, can be written as $f = \sum_{i=1}^n c_i \kappa(\mathbf{x}_i, \cdot)$. Thus the vector $(f(\mathbf{x}_1), \dots, f(\mathbf{x}_n)) = \bar{c}K$, where $\bar{c} = (c_1, \dots, c_n)$. The components of (2.15) can be rewritten in terms of the Gram matrix K and the coefficient \bar{c} as

$$n^{-1} \sum_{i=1}^n |\bar{A}_i - f(\mathbf{x}_i)|^2 = n^{-1} \|\bar{A} - \bar{c}K\|_{\mathbb{R}^n}^2,$$

and

$$\begin{aligned}\lambda_1 \|f\|_{\mathcal{W}}^2 &= \lambda_1 \left\langle \sum_{i=1}^n c_i \kappa(\mathbf{x}_i, \cdot), \sum_{j=1}^n c_j \kappa(\mathbf{x}_j, \cdot) \right\rangle_{\mathcal{W}} \\ &= \lambda_1 \sum_{i,j=1}^n c_i c_j \kappa(\mathbf{x}_i, \mathbf{x}_j) = \lambda_1 \langle \bar{c}K, \bar{c} \rangle_{\mathbb{R}^n},\end{aligned}$$

where $\bar{A} = (\bar{A}_1, \dots, \bar{A}_n)$ and we have used the symmetry property of the kernel function. This allows us to consider the optimization problem (2.15) as a function of \bar{c} admitting a representation,

$$\begin{aligned}\mathcal{M}(\bar{c}) &:= n^{-1} \sum_{i=1}^n |\bar{A}_i - f(\mathbf{x}_i)|^2 + \lambda_1 \|f\|_{\mathcal{W}}^2 = n^{-1} \|\bar{A} - \bar{c}K\|_{\mathbb{R}^n}^2 + \lambda_1 \langle \bar{c}K, \bar{c} \rangle_{\mathbb{R}^n} \\ &= n^{-1} \|\bar{A}\|_{\mathbb{R}^n}^2 - 2n^{-1} \langle \bar{c}, \bar{A}K \rangle_{\mathbb{R}^n} + \langle \bar{c}, \bar{c}(\lambda_1 K + n^{-1}K^2) \rangle_{\mathbb{R}^n},\end{aligned}\tag{2.18}$$

where in the last equality we use the fact that K is a symmetric matrix. By the representer theorem, if the minimizer of the problem (2.15) has the form of the equation (2.17), then the vector $\bar{c}^* = (c_1^*, \dots, c_n^*)$ satisfies

$$\nabla_{\bar{c}} \mathcal{M}(\bar{c}) = -2n^{-1} \bar{A}K + 2\bar{c}K(\lambda_1 I + n^{-1}K) = 0,\tag{2.19}$$

for $\bar{c} = \bar{c}^*$. Since the kernel function κ is a positive semidefinite function, then the Gram matrix K is a singular matrix. Thus, we obtain the formula for \bar{c}^* :

$$\bar{c}^* = \bar{A}K[K(n\lambda_1 I + K)]^\dagger,\tag{2.20}$$

where $[K(n\lambda_1 I + K)]^\dagger$ is the generalized inverse of the matrix $[K(n\lambda_1 I + K)]$.

Analogously, the minimizer of problem (2.16) is given by $\psi^*(\cdot) = \sum_{i=1}^n \bar{e}_i^* \kappa(\mathbf{x}_i, \cdot)$, and

$$\bar{e}^* = \hat{A}K[K(n\lambda_2 I + K)]^\dagger, \quad \hat{A} = (\hat{A}_1, \dots, \hat{A}_n).\tag{2.21}$$

We have now gathered all the ingredients needed to approximate the scattering amplitude A . Then for a random point $\mathbf{t} = (t_1, t_2, t_3, t_4)$ in \mathbb{R}^4 , we approximate A by

$$F(\mathbf{t}) = f(\mathbf{t}) + i\psi(\mathbf{t}) = \sum_{i=1}^n \bar{\beta}_i^* \kappa(\mathbf{x}_i, \mathbf{t}),\tag{2.22}$$

where $\mathbf{x}_i \in \mathcal{D}$, and

$$\bar{\beta}^* := \bar{c}^* + i\bar{e}^*,\tag{2.23}$$

with \bar{c}^* , \bar{e}^* are as in (2.20) and (2.21). The reconstruction of the susceptibility η via (2.10) requires differentiation of $A(\mathbf{r}_1, \mathbf{r}_2)$ with respect to \mathbf{r}_1 , which in turn requires differentiation of $F(t_1, t_2, t_3, t_4)$ with respect to the first two components t_1 and t_2 , yielding

$$\Delta_{t_1, t_2} F(\mathbf{t}) = \sum_{i=1}^n \bar{\beta}_i^* \kappa''(\mathbf{x}_i, \mathbf{t}),\tag{2.24}$$

where $\kappa''(\mathbf{x}, \mathbf{t})$ is given by

$$\kappa''(\mathbf{x}, \mathbf{t}) = -4\pi^2 \int_{\mathbb{R}^4} \frac{(u_1^2 + u_2^2) \prod_{j=1}^4 \cos(2\pi(x_j - t_j)u_j)}{(1 + \sum_{0 < |\alpha| \leq 3} \prod_{j=1}^4 (2\pi u_j)^{2\alpha_j})} d\mathbf{u}.$$

2.3. Three dimensional problem. We consider next the case of a three-dimensional medium. The total field U still satisfies the time-harmonic wave equation (2.1) and the integral equation (2.2), but the three-dimensional Green's function is given by

$$G(\mathbf{r}, \mathbf{r}') = \frac{e^{ik|\mathbf{r} - \mathbf{r}'|}}{4\pi|\mathbf{r} - \mathbf{r}'|}.$$

In the far field, the Green's function takes the asymptotic form for $\mathbf{r} \gg \mathbf{r}'$ given by,

$$G(\mathbf{r}, \mathbf{r}') = \frac{e^{ik|\mathbf{r}|}}{4\pi|\mathbf{r}|} \left(e^{-ik\hat{\mathbf{r}} \cdot \mathbf{r}'} + \mathcal{O}\left(\frac{1}{|\mathbf{r}|}\right) \right). \quad (2.25)$$

It follows that the asymptotic behavior of the total field is given by,

$$\begin{aligned} U(\mathbf{r}) &= a(\mathbf{r}_1) G(\mathbf{r}, \mathbf{r}_1) + k^2 \int G(\mathbf{r}, \mathbf{r}') \eta(\mathbf{r}') U(\mathbf{r}') d\mathbf{r}' \\ &\sim \frac{e^{ik|\mathbf{r}|}}{4\pi|\mathbf{r}|} \left(a(\mathbf{r}_1) e^{-ik\hat{\mathbf{r}} \cdot \mathbf{r}_1} + k^2 \int e^{-ik\hat{\mathbf{r}} \cdot \mathbf{r}'} \eta(\mathbf{r}') U(\mathbf{r}') d\mathbf{r}' \right). \end{aligned}$$

In the far-zone of the scatterer, the field behaves as an outgoing spherical wave:

$$U(\mathbf{r}) \sim \frac{e^{ik|\mathbf{r}|}}{4\pi|\mathbf{r}|} \left(a(\mathbf{r}_1) e^{-ik\hat{\mathbf{r}} \cdot \mathbf{r}_1} + A(\mathbf{r}) \right), \quad (2.26)$$

where the scattering amplitude A is defined by

$$A(\mathbf{r}) = k^2 \int_{\Omega} e^{-ik\hat{\mathbf{r}} \cdot \mathbf{r}'} \eta(\mathbf{r}') U(\mathbf{r}') d\mathbf{r}'. \quad (2.27)$$

Following the same procedure as before, the scattering amplitude in three dimensions is rewritten as,

$$A(\mathbf{r}_1, \mathbf{r}_2) = a(\mathbf{r}_1) k^2 \int_{\Omega} e^{-ik\hat{\mathbf{r}}_2 \cdot \mathbf{r}} \eta(\mathbf{r}) G(\mathbf{r}, \mathbf{r}_1) d\mathbf{r}, \quad (2.28)$$

where we assume that the sources have unit amplitude. The inversion formula for η is thus given by,

$$\eta(\mathbf{r}_1; \mathbf{r}_2) = -\frac{e^{ik\hat{\mathbf{r}}_2 \cdot \mathbf{r}_1}}{k^2} \left(\Delta_{\mathbf{r}_1} A(\mathbf{r}_1, \mathbf{r}_2) + k^2 A(\mathbf{r}_1, \mathbf{r}_2) \right). \quad (2.29)$$

The three-dimensional inverse problems are also considered in [9], where (2.28) is converted into a linear system and then a regularized pseudoinverse solution is used to recover the susceptibility. In addition, the number of sources, detectors, and volume elements in Ω was chosen so that the resulting linear system is overdetermined. Moreover, the two-dimensional case was not considered in [9].

The forward problem of solving (2.28) was carried out by using the coupled-dipole method [14, 19]. We discretized the three-dimensional domain Ω into voxels C_m ($m = 1, 2, \dots, N_\nu$) of volume h^3 , where N_ν is the total number of voxels. We make the following approximation:

$$\eta(\mathbf{r}) = \eta(\tilde{\mathbf{r}}_m), \quad \text{if } \mathbf{r} \in C_m,$$

where $\tilde{\mathbf{r}}_m$ is the central point of the respective voxels C_m . We split the integral of (2.28) into singular- and non-singular parts according to

$$\int_{\Omega} e^{-ik\hat{\mathbf{r}}_2 \cdot \mathbf{r}} \eta(\mathbf{r}) G(\mathbf{r}, \mathbf{r}_1) d\mathbf{r} = \sum_{m=1}^{N_\nu} \int_{C_m \setminus C_n} e^{-ik\hat{\mathbf{r}}_2 \cdot \mathbf{r}} \eta(\mathbf{r}) G(\mathbf{r}, \mathbf{r}_1) d\mathbf{r} + \int_{C_n} e^{-ik\hat{\mathbf{r}}_2 \cdot \mathbf{r}} \eta(\mathbf{r}) G(\mathbf{r}, \mathbf{r}_1) d\mathbf{r}, \quad (2.30)$$

where C_n is the voxel containing the singularity. We assume that $kh \ll 1$. Combining the fact that $e^{ik|\mathbf{r} - \mathbf{r}_1|} \approx 1 + ik|\mathbf{r} - \mathbf{r}_1|$, the singular part of (2.30) is computed as

$$\int_{\mathbf{r} \in C_n} e^{-ik\hat{\mathbf{r}}_2 \cdot \mathbf{r}} \eta(\mathbf{r}) G(\mathbf{r}, \mathbf{r}_1) d\mathbf{r} \approx \frac{1}{4\pi} \eta(\tilde{\mathbf{r}}_n) e^{-ik\hat{\mathbf{r}}_2 \cdot \tilde{\mathbf{r}}_n} \int_{-\frac{h}{2}}^{\frac{h}{2}} \int_{-\frac{h}{2}}^{\frac{h}{2}} \int_{-\frac{h}{2}}^{\frac{h}{2}} \left(\frac{1}{|\mathbf{r} - \mathbf{r}_1|} + ik \right) d\mathbf{r} = \frac{1}{4\pi} \eta(\tilde{\mathbf{r}}_n) e^{-ik\hat{\mathbf{r}}_2 \cdot \tilde{\mathbf{r}}_n} \zeta, \quad (2.31)$$

where $\zeta = h^2(\xi + ikh)$ with $\xi = \ln(26 + 15\sqrt{3}) - \frac{\pi}{2} \approx 2.38$, and $\tilde{\mathbf{r}}_n$ is the central point in C_n .

For the non-singular part of (2.30), we have for $m \neq n$:

$$\int_{\mathbf{r} \in C_m} e^{-ik\hat{\mathbf{r}}_2 \cdot \mathbf{r}} \eta(\mathbf{r}) G(\mathbf{r}, \mathbf{r}_1) d\mathbf{r} \approx h^3 \eta(\tilde{\mathbf{r}}_m) e^{-ik\hat{\mathbf{r}}_2 \cdot \tilde{\mathbf{r}}_m} G(\tilde{\mathbf{r}}_m, \mathbf{r}_1),$$

where $\tilde{\mathbf{r}}_m$ is the central point in voxel C_m ($m \neq n$).

Following along similar lines as in the previous subsection, we reconstruct the three-dimensional susceptibility η based on (2.29). We consider the optimization problems (2.15) and (2.16) in the Sobolev space $W_2^s(\mathbb{R}^d)$, where $d = 6$ and $s = 4$, which is a RKHS. The space $W_2^4(\mathbb{R}^6)$ has the reproducing kernel given by [17]:

$$\kappa(\mathbf{x}, \mathbf{t}) = \int_{\mathbb{R}^6} \frac{\prod_{j=1}^6 \cos(2\pi(x_j - t_j)u_j)}{(1 + \sum_{0 < |\alpha|_1 \leq 4} \prod_{j=1}^6 (2\pi u_j)^{2\alpha_j})} d\mathbf{u}, \quad (2.32)$$

where $\mathbf{x} = (\mathbf{r}_1, \mathbf{r}_2) \in \mathbb{R}^6$ with \mathbf{r}_1 and \mathbf{r}_2 are the source and detector positions, respectively, and $|\alpha|_1 = \sum_{j=1}^6 \alpha_j$ with non-negative integers α_j . Similarly, we identify functionals f and ψ in the RKHS $W_2^4(\mathbb{R}^6)$ that approximate the real part and the imaginary part of the scattering amplitude A , respectively. Thus, we approximate the scattering amplitude A by $F(\mathbf{t}) = \sum_{i=1}^n \bar{\beta}_i^* \kappa(\mathbf{x}_i, \mathbf{t})$, where $\mathbf{t} = (t_1, t_2, t_3, t_4, t_5, t_6)$ is a random point in \mathbb{R}^6 , $\mathbf{x}_i \in \mathcal{D}$ and $\bar{\beta}_i^*$ as in (2.23). The reconstruction of η from (2.29) requires differentiation of $A(\mathbf{r}_1, \mathbf{r}_2)$ with respect to \mathbf{r}_1 , which in turn requires differentiation of $F(t_1, t_2, t_3, t_4, t_5, t_6)$ with respect to t_1, t_2 and t_3 , yielding

$$\Delta_{t_1, t_2, t_3} F(\mathbf{t}) = \sum_{i=1}^n \bar{\beta}_i^* \kappa''(\mathbf{x}_i, \mathbf{t}), \quad (2.33)$$

where $\kappa''(\mathbf{x}, \mathbf{t})$ is given by

$$\kappa''(\mathbf{x}, \mathbf{t}) = \int_{\mathbb{R}^6} \frac{-4\pi^2 (\sum_{i=1}^3 u_i^2) \prod_{j=1}^6 \cos(2\pi(x_j - t_j)u_j)}{(1 + \sum_{0 < |\alpha|_1 \leq 4} \prod_{j=1}^6 (2\pi u_j)^{2\alpha_j})} d\mathbf{u}.$$

Finally, following the same procedure as in the previous subsection, we reconstruct η using (2.29).

For three-dimensional reconstructions, we present two methods. First we perform two-dimensional reconstructions using (2.10) for each slice, and then make a three-dimensional reconstruction by assembling these cross-sectional reconstructions together. The second, is to directly use (2.29) for three-dimensional reconstruction.

3. NUMERICAL EXPERIMENTS

In this section, we present the numerical reconstruction of the susceptibility. To better illustrate the method we consider the two-dimensional case as an example.

For a random point $\mathbf{t} = (t_1, t_2, t_3, t_4) \in \mathbb{R}^4$, let $(t_1, t_2) = \mathbf{r}'_1$ and $(t_3, t_4) = \mathbf{r}'_2$, we approximate the scattering amplitude $A(\mathbf{t})$ by $A(\mathbf{t}) \approx \sum_{i=1}^n \bar{\beta}_i^* \kappa(\mathbf{x}_i, \mathbf{t})$, where $\mathbf{x}_i \in \mathcal{D}$, κ is the reproducing kernel in (2.14), and $\bar{\beta}_i^*$ as in (2.23). Then by (2.24), the differentiation of $A(\mathbf{t})$ with respect to $\mathbf{r}'_1 = (t_1, t_2)$ is given by $\Delta_{\mathbf{r}'_1} A(\mathbf{t}) \approx \sum_{i=1}^n \bar{\beta}_i^* \kappa''(\mathbf{x}_i, \mathbf{t})$. Thus by (2.10), we derive one susceptibility reconstruction at $\mathbf{r}'_1 = (t_1, t_2)$ of the medium:

$$\eta(\mathbf{r}'_1; \mathbf{r}'_2) = -\frac{e^{ik\hat{\mathbf{r}}_2 \cdot \mathbf{r}'_1}}{k^{\frac{3}{2}}} (\Delta_{\mathbf{r}'_1} A(\mathbf{r}'_1, \mathbf{r}'_2) + k^2 A(\mathbf{r}'_1, \mathbf{r}'_2)) \approx -\frac{e^{ik\hat{\mathbf{r}}_2 \cdot \mathbf{r}'_1}}{k^{\frac{3}{2}}} \sum_{i=1}^n \bar{\beta}_i^* (\kappa''(\mathbf{x}_i, \mathbf{t}) + \kappa(\mathbf{x}_i, \mathbf{t})).$$

If we have multiple $\mathbf{r}'_2 = (t_3, t_4)$ for the above susceptibility reconstruction, we take the average of the reconstructions according to (2.11).

With these preparations, we present three numerical experiments.

3.1. Reconstructions of a three-ball model. We consider reconstructing a three-ball model [9]. The model system consists of a volume of dimensions $70 \text{ nm} \times 70 \text{ nm} \times 40 \text{ nm}$. Three spherical scatterers of radius 12 nm are placed so their lowest point is 3 nm from the bottom of the sample. The minimum distance between any two spheres is 5 nm . The susceptibility of two of the spheres is set to 1.275 , while the remaining sphere has a susceptibility of 1.885 . The background has a susceptibility of 0 . The wave number is given by $k = 2\pi/500 = 0.0126$. We divide the system into 19 layers, with each layer being a two-dimensional medium. We solve the forward problem on each layer with a discretization of 35×35 . Gaussian noise at the 1% level is then added to the scattering amplitude and the positions of the sources. Then the susceptibility for each layer is subsequently reconstructed on a grid of size 31×31 by (2.10). The regularization parameters for calculating (2.23) are set to be 10^{-10} for each layer. This model system is

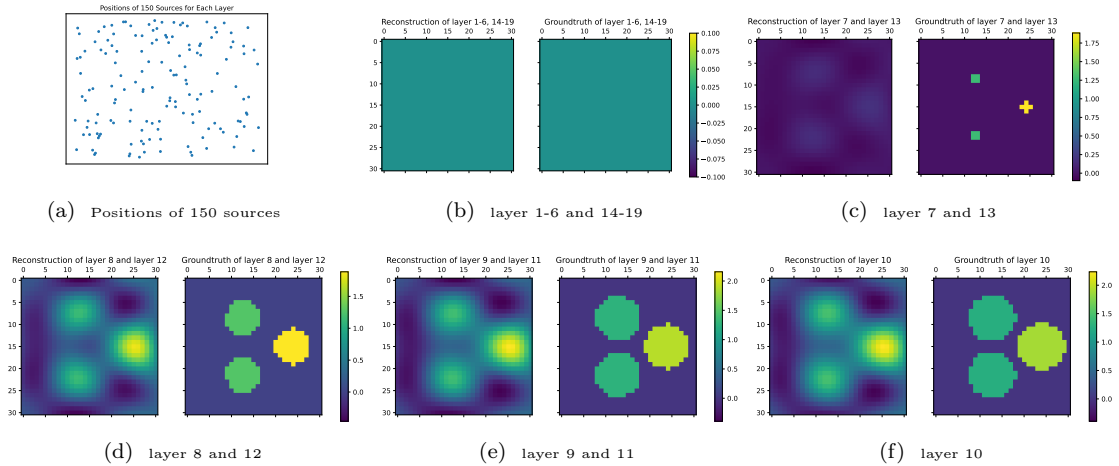


FIGURE 1. *Susceptibility reconstruction of three spherical scatterers on each layer by the two-dimensional method.*

similar to what is considered in [9]. We use 150 randomly placed sources and 7 detectors of L shape in this experiment, for each layer, to show the feasibility of the two-dimensional reconstruction method.

Figure 1 shows the position of the sources and the reconstructions for each layer. Due to the symmetry of the medium and the source positions for each layer being the same, some layer reconstructions are also identical. In our three-ball model, layer 10 is the central layer, so layers 8 & 12, and layers 9 & 11 (see Figure 1 (d) & (e)) yield identical reconstructions. Thus, one can reconstruct either of the two layers, hence reducing the reconstruction time. It is also worth noting that the Gram matrix K for each layer is the same since the positions of the sources, detectors and the reconstruction grid are the same for each layer. This also applies to subsection 3.2.1.

3.2. Reconstructions of a neuron. We consider a neuron from a rat brain, of size $3.928 \mu\text{m} \times 5.44 \mu\text{m} \times 2.248 \mu\text{m}$. The image was obtained from the experiment and manually segmented [15, 16]. The main trunk of the neuron has a susceptibility of $\eta = 0.25$ and the branches spines have a susceptibility of $\eta = 0.38$, while the background has susceptibility $\eta = 0$. Once again, 1% Gaussian noise is added to the scattering amplitude and the positions of the sources. Both two-dimensional method and three-dimensional methods were tested.

3.2.1 Two-dimensional reconstruction method

We manually segmented the neuron into a grid of size $33 \times 46 \times 18$, then we calculated the forward problem on 18 layers with each layer of size 33×46 . Subsequently, we reconstructed each of these 18 layers onto a 31×44 grid, denoted as $\mathcal{G} := \{(g_i, g_j)\}$, with $i = 1, \dots, 31$, and $j = 1, \dots, 44$. For each layer, 500 randomly spaced sources and 7 detectors were employed. The regularization parameters for calculating (2.23) are set to be 5×10^{-10} for each layer.

Since we approximate the scattering amplitude A by $F(\mathbf{t})$ via (2.22), for $\mathbf{t} = (t_1, t_2, t_3, t_4) \in \mathbb{R}^4$, we can approximate the value at grid points by letting $(t_1, t_2) = (g_i, g_j)$ and randomly set (t_3, t_4) . In Figure 2, we only set one (t_3, t_4) , which is the coordinate of one detector, yielding one susceptibility reconstruction for each grid point.

Then putting all of the layers together, we obtain the reconstruction shown in Figure 3. To better display the three-dimensional colour map, we add transparency to the points of value less than 0.085.

Let us define the relative error for A :

$$\chi^2 = \frac{\sum_{\mathbf{r}_1, \mathbf{r}_2} |A(\mathbf{r}_1, \mathbf{r}_2) - F(\mathbf{r}_1, \mathbf{r}_2)|^2}{\sum_{\mathbf{r}_1, \mathbf{r}_2} |A(\mathbf{r}_1, \mathbf{r}_2)|^2},$$

where $F(\mathbf{r}_1, \mathbf{r}_2)$ is the reconstructed scattering amplitude at $(\mathbf{r}_1, \mathbf{r}_2) \in \mathcal{D}$. We define the mean relative

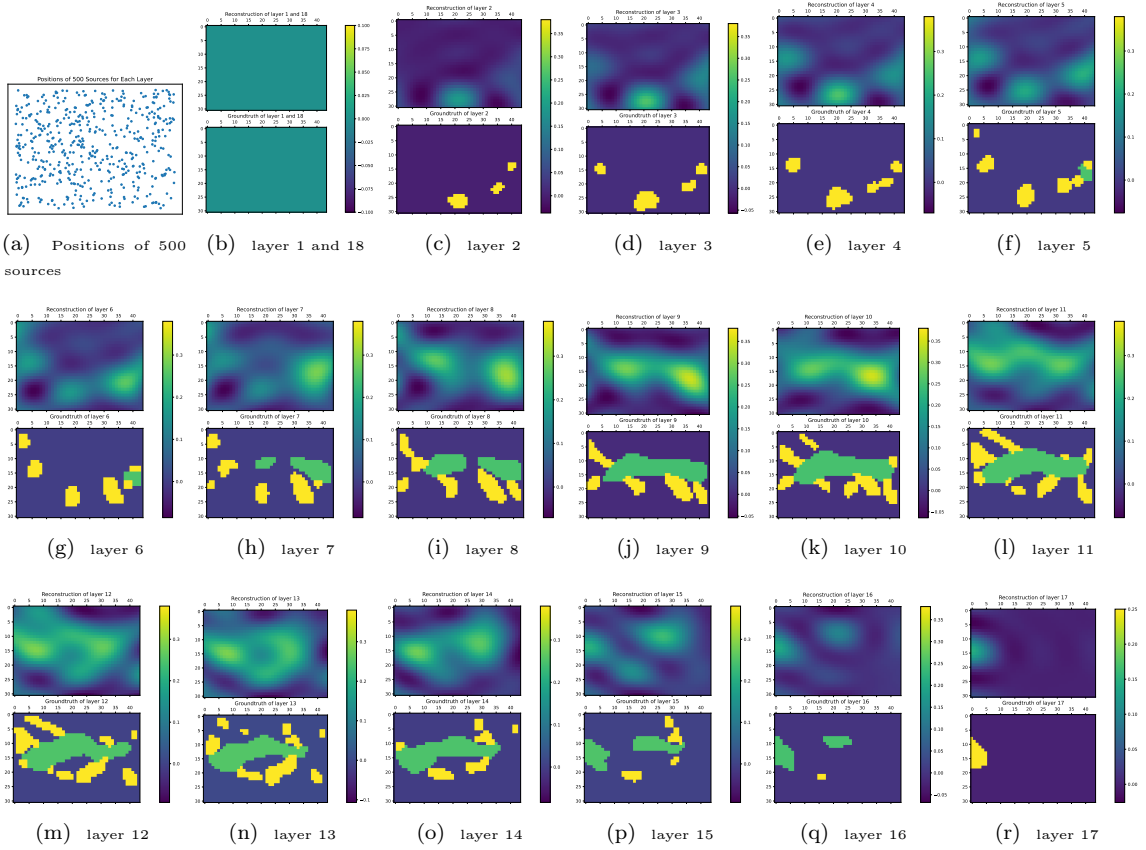


FIGURE 2. Neuron model and susceptibility reconstructions on each layer by the two-dimensional method.

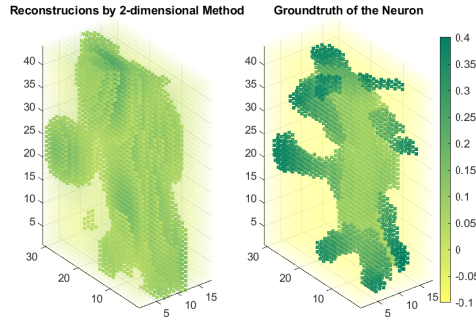


FIGURE 3. Neuron reconstructions by two-dimensional method compared to the groundtruth.

error of the susceptibility at grid \mathcal{G} as

$$\delta = \frac{\sum_{i=1}^{31} \sum_{j=1}^{44} |\eta\{g_i, g_j\} - \eta_{rec}\{g_i, g_j\}|}{31 \times 44},$$

where, $\eta\{g_i, g_j\}$ is the groundtruth susceptibility at grid point (g_i, g_j) , and η_{rec} is the reconstructed susceptibility.

It is important to determine the optimal number of detectors, sources and (t_3, t_4) for a given experiment. In Figure 4 we employ 7 detectors and show the behavior of the error with different numbers of sources on the reconstructions of layer 9. We set (t_3, t_4) equal to the coordinates of 7 detectors, which leads to multiple reconstructions of susceptibility. Then the mean of the multiple reconstructions compared to the single (t_3, t_4) reconstruction is plotted. We see that using 500 sources almost reaches the minimum of the

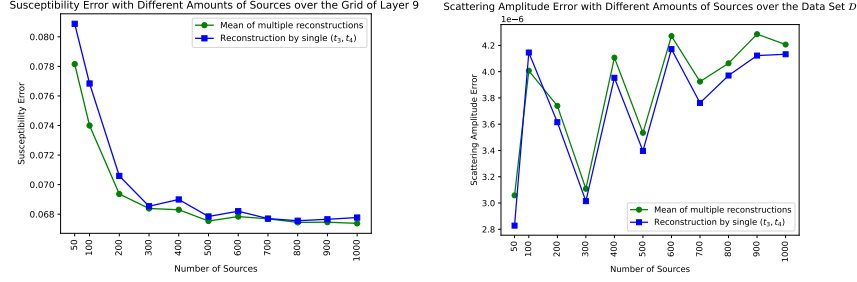


FIGURE 4. Error behavior with different numbers of sources

susceptibility error. Moreover, the reconstructed susceptibility error by a single (t_3, t_4) is comparable to multiple detectors. Thus, Figure 4 shows that one can choose 500 sources and single (t_3, t_4) .

Next, in Figure 5, we fix 500 sources and choose a single (t_3, t_4) reconstruction for each grid point, we then test the impact of different numbers of detectors on the reconstructions. We find that the number of detectors does not significantly affect the susceptibility reconstructions. In all settings (Figure 4 and Figure 5), the scattering amplitude error is on the order of 10^{-6} . This shows good performance of using the RKHS method. Note that the reconstructions depicted in Figure 2 have been obtained using the same configuration of 500 sources, 7 detectors, and single (t_3, t_4) as those also utilized in Figure 4 and Figure 5.

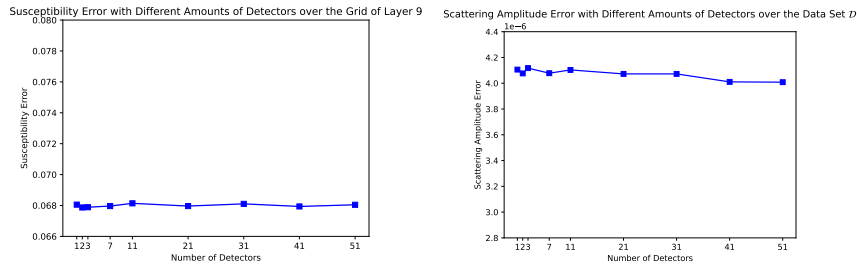


FIGURE 5. Error behavior using different numbers of detectors

3.2.2 Three-dimensional reconstruction method

Here we show the feasibility of our three-dimensional reconstruction method and compare the reconstructions with known results. We segment the neuron into a grid of size $33 \times 46 \times 19$, and then we solve the forward problem on this grid with 500 randomly spaced sources and 7 detectors. Subsequently, we reconstruct the model on the grid $31 \times 44 \times 18$, thus, avoiding an inverse crime. The regularization parameters for calculating (2.23) are set to be 10^{-11} . The susceptibility reconstruction is shown in Figure 6, where the purple dots indicate the positions of the sources. Once again, we add transparency to the points of value less than 0.08 to better display the color map.

We next compared our RKHS method with the method in [9]. We consider the same problem setting as in [9] and compute the corresponding scattering amplitude error results in Table 1. The regularization parameters for our RKHS method are all set to be 10^{-11} . We see that for setup in [9], the scattering amplitude error by the proposed method is less than reported in [9]. Moreover, one can reduce the number of detectors from 225 to 7 and still obtain the same scattering amplitude error. Thus the proposed RKHS method is superior to the method presented in [9].

Furthermore, Table 1 also contains the susceptibility error computed from our RKHS method. We observe that the susceptibility error for the 225 detectors case is comparable with the case of 7 detectors. Thus one can reduce the number of detectors from 225 to 7 and still reach the same level of susceptibility error.

TABLE 1. Comparison between our RKHS method and the one reported in [9].

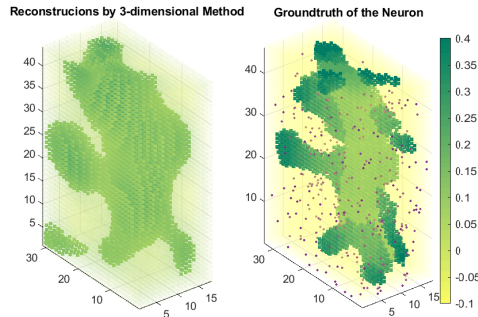


FIGURE 6. Neuron reconstructions by the three-dimensional method compared to groundtruth.

	Linear system [9]	RKHS method	RKHS method
Number of sources	500	500	500
Number of detectors	225	225	7
Discretization of the forward problem	$33 \times 46 \times 19$	$33 \times 46 \times 19$	$33 \times 46 \times 19$
Scattering amplitude error	1×10^{-2}	1.3×10^{-4}	1.2×10^{-4}
Susceptibility error	Not provided	5.8×10^{-2}	6.0×10^{-2}

The source code is available on Gitlab at the following link: https://gitlab.com/csc1/cisis-rkhs/-/tree/master/ISP_RKHS_YDong_code?ref_type=heads. The discrete three-ball model and discrete neuron model are presented at the following link: <https://phaidra.univie.ac.at/o:2085789>.

4. CONCLUSION

We have developed a method to reconstruct the dielectric susceptibility of an inhomogeneous scattering medium from internal sources using a RKHS approach. Our numerical results in two- and three-dimensional problems exhibit better performance compared to previous work in [9]. We note that the approach we have presented is quite general and applicable to imaging with any scalar wave field with internal sources.

Acknowledgements. This research was funded in whole, or in part, by the Austrian Science Fund (FWF) 10.55776/P34981 (OS & YD) – New Inverse Problems of Super-Resolved Microscopy (NIPSUM), SFB 10.55776/F68 (OS) “Tomography Across the Scales,” project F6807-N36 (Tomography with Uncertainties). The financial support by the Austrian Federal Ministry for Digital and Economic Affairs, the National Foundation for Research, Technology and Development and the Christian Doppler Research Association is gratefully acknowledged. The work of JCS was supported by NSF grant DMS-1912821 and AFOSR grant FA9550-19-1-0320. For the purpose of open access, the author has applied a CC BY public copyright license to any Author Accepted Manuscript version arising from this submission. The computational results presented have been achieved using the Vienna Scientific Cluster (VSC).

REFERENCES

- [1] N. Aronszajn. “Theory of reproducing kernels”. In: *Transactions of the American Mathematical Society* 68.3 (1950), pp. 337–404. DOI: [10.1090/s0002-9947-1950-0051437-7](https://doi.org/10.1090/s0002-9947-1950-0051437-7) (cited on pages 1, 4).
- [2] E. Betzig, G. H. Patterson, R. Sougrat, O. W. Lindwasser, S. Olenych, J. S. Bonifacino, M. W. Davidson, J. Lippincott-Schwartz, and H. F. Hess. “Imaging intracellular fluorescent proteins at nanometer resolution”. In: *Science* 313.5793 (2006), pp. 1642–1645. ISSN: 0036-8075. DOI: [10.1126/science.1127344](https://doi.org/10.1126/science.1127344) (cited on page 1).
- [3] M. Born and E. Wolf. “Principles of Optics”. 7th ed. Cambridge: Cambridge University Press, 1999 (cited on page 2).

-
- [4] R. Carminati and J. C. Schotland. “Principles of Scattering and Transport of Light”. Cambridge University Press, 2021. DOI: [10.1017/9781316544693](https://doi.org/10.1017/9781316544693) (cited on pages 1, 2).
- [5] D. Colton and R. Kress. “Inverse acoustic and electromagnetic scattering theory”. 2nd ed. Vol. 93. Applied Mathematical Sciences. Berlin: Springer-Verlag, 1998. xii+334. ISBN: 3-540-62838-X (cited on page 2).
- [6] H. W. Engl, M. Hanke, and A. Neubauer. “Regularization of inverse problems”. Mathematics and its Applications 375. Dordrecht: Kluwer Academic Publishers Group, 1996. viii+321. ISBN: 0-7923-4157-0 (cited on page 1).
- [7] C. L. Epstein. “Introduction to the Mathematics of Medical Imaging”. New York: Prentice Hall, 2003 (cited on page 1).
- [8] C. Errico, J. Pierre, S. Pezet, Y. Desailly, Z. Lenkei, O. Couture, and M. Tanter. “Ultrafast ultrasound localization microscopy for deep super-resolution vascular imaging”. In: *Nature* 527.7579 (2015), pp. 499–502. DOI: [10.1038/nature16066](https://doi.org/10.1038/nature16066) (cited on page 1).
- [9] A. C. Gilbert, H. W. Levinson, and J. C. Schotland. “Imaging from the inside out: inverse scattering with photoactivated internal sources”. In: *Optics Letters* 43.12 (2018), p. 3005. DOI: [10.1364/ol.43.003005](https://doi.org/10.1364/ol.43.003005) (cited on pages 1, 6–8, 10, 11).
- [10] S. W. Hell et al. “The 2015 super-resolution microscopy roadmap”. In: *Journal of Physics D: Applied Physics* 48.44 (2015), p. 443001. DOI: [10.1088/0022-3727/48/44/443001](https://doi.org/10.1088/0022-3727/48/44/443001) (cited on page 1).
- [11] G. Kimeldorf and G. Wahba. “Some results on Tchebycheffian spline functions”. In: *Journal of Mathematical Analysis and Applications* 33.1 (1971), pp. 82–95. ISSN: 0022-247X. DOI: [10.1016/0022-247x\(71\)90184-3](https://doi.org/10.1016/0022-247x(71)90184-3) (cited on page 4).
- [12] G. S. Kimeldorf and G. Wahba. “A Correspondence Between Bayesian Estimation on Stochastic Processes and Smoothing by Splines”. In: *The Annals of Mathematical Statistics* 41.2 (1970), pp. 495–502. DOI: [10.1214/aoms/1177697089](https://doi.org/10.1214/aoms/1177697089) (cited on pages 1, 4).
- [13] P. Kuchment. “The Radon Transform and Medical Imaging”. CBMS-NSF Regional Conference Series in Applied Mathematics. Philadelphia: SIAM, 2013. DOI: [10.1137/1.9781611973297](https://doi.org/10.1137/1.9781611973297) (cited on page 1).
- [14] H. W. Levinson and V. A. Markel. “Solution of the nonlinear inverse scattering problem by T-matrix completion. I. Theory”. In: *Physical Review E* 94.4 (2016). DOI: [10.1103/physreve.94.043317](https://doi.org/10.1103/physreve.94.043317) (cited on page 6).
- [15] M. E. Martone, T. J. Deerinck, N. Yamada, E. Bushong, and M. H. Ellisman. “Correlated 3D Light and Electron Microscopy: Use of High Voltage Electron Microscopy and Electron Tomography for Imaging Large Biological Structures”. In: *Journal of Histotechnology* 23.3 (2000), pp. 261–270. DOI: [10.1179/his.2000.23.3.261](https://doi.org/10.1179/his.2000.23.3.261) (cited on page 8).
- [16] M. E. Martone, A. Gupta, M. Wong, X. Qian, G. Sosinsky, B. Ludäscher, and M. H. Ellisman. “A cell-centered database for electron tomographic data”. In: *Journal of Structural Biology* 138.1-2 (2002), pp. 145–155. DOI: [10.1016/s1047-8477\(02\)00006-0](https://doi.org/10.1016/s1047-8477(02)00006-0) (cited on page 8).
- [17] E. Novak, M. Ullrich, H. Woźniakowski, and S. Zhang. “Reproducing kernels of Sobolev spaces on \mathbb{R}^d and applications to embedding constants and tractability”. In: *Analysis and Applications* 16.5 (2018), pp. 693–715. DOI: [10.1142/s0219530518500094](https://doi.org/10.1142/s0219530518500094) (cited on pages 4, 7).
- [18] S. Pereverzyev. “An Introduction to Artificial Intelligence Based on Reproducing Kernel Hilbert Spaces”. 2022. DOI: [10.1007/978-3-030-98316-1](https://doi.org/10.1007/978-3-030-98316-1) (cited on page 4).
- [19] E. M. Purcell and C. R. Pennypacker. “Scattering and Absorption of Light by Nonspherical Dielectric Grains”. In: *The Astrophysical Journal* 186 (1973), pp. 705–714. DOI: [10.1086/152538](https://doi.org/10.1086/152538) (cited on page 6).
- [20] S. Saitoh and Y. Sawano. “Theory of Reproducing Kernels and Applications”. 2016. DOI: [10.1007/978-981-10-0530-5](https://doi.org/10.1007/978-981-10-0530-5) (cited on page 4).
- [21] A. N. Tikhonov and V. Y. Arsenin. “Solutions of Ill-Posed Problems”. Washington, D.C.: John Wiley & Sons, 1977 (cited on page 1).
- [22] A. B. Weglein, F. V. Araújo, P. M. Carvalho, R. H. Stolt, K. H. Matson, R. T. Coates, D. Corrigan, D. J. Foster, S. A. Shaw, and H. Zhang. “Inverse scattering series and seismic exploration”. In: *Inverse Problems* 19.6 (2003), R27–R83. ISSN: 0266-5611. DOI: [10.1088/0266-5611/19/6/r01](https://doi.org/10.1088/0266-5611/19/6/r01) (cited on page 1).